scientific reports

Check for updates

OPEN

Deformation mechanism of soft rock based on mineral crystal models

Bo Wang[1], Qihua Zhao[1]✉, Guangchuan Liang[1], Bing Lan[2] & Lu Lu[3]

To investigate the influence of microstructural heterogeneity on rock deformation and failure mechanisms, this study first analyzes the mineral composition of mudstone and obtains its mechanical parameters through laboratory testing. Subsequently, establishing a particle flow code-grain based model (PFC-GBM) to simulate the microstructure of mudstone, calibrated with experimental parameters. The influences of the proportion of clay minerals, and mineral crystal size on crack evolution and crack distribution during mudstone failure are investigated. The results demonstrate that: (1) Clay mineral crystals experience initial damage during mudstone failure, followed by relative movement between mineral crystals, leading to a significant number of cracks. Shear failure dominates the process, with shear cracks and intercrystalline cracks accounting for 61.3% and 52.7% of total cracks, respectively. (2) With an increase in the proportion of clay mineral crystals, both peak strength and damage strength of mudstone decrease, with peak strength dropping from 11.95 MPa to 9.13 MPa. Furthermore, the location of crack generation shifts from the center towards the two ends of the sample post-failure. (3) The size of the mineral crystals in mudstone primarily influences the generation of intercrystalline cracks. As the mineral crystal size decreases, cracks in the mudstone gradually propagate toward the center of the mudstone after failure, with intercrystalline cracks increasing from 25.3 to 51.5%. This study primarily simulates microstructural evolution at the mineral crystal scale in heterogeneous soft rocks, providing deeper insights into the deformation and failure characteristics of soft rocks. The findings offer valuable reference points for understanding the stability of soft rock slopes.

Keywords Heterogeneous rocks, PFC-GBM, Deformation mechanism, Crack evolution

Natural rocks, formed through complex geological and tectonic processes, exhibit significant heterogeneity due to variations in their formation period and environmental conditions. This heterogeneity is evident in differences in rock structure, types of cementing materials, proportions of mineral crystal components, and the geometric sizes of these components. When subjected to external forces, rocks undergo failure, and micro-cracks mainly form in two ways (Fig. 1): (1) grain boundary failure cracks that occur along the contact interfaces of various mineral crystals; (2) Intra-crystalline failure cracks that penetrate within the mineral crystals. Therefore, analyzing the impact of differences in rock mineral crystal compositions on rock deformation and failure is of significant importance for the stability of slopes, underground projects, and similar structures.

In recent years, numerous scholars have studied the impact of the mesostructure of mineral crystal compositions on the mechanical behavior of rocks, conducting extensive experiments and theoretical analyses. Hallbauer et al.[3] were among the first to propose that during the rock failure process, the particles of mineral crystals cause uneven stress distribution, leading to internal stress concentration and affecting the failure mode of rocks. Wong et al.[4] suggested that the particle size of mineral crystal components is inversely proportional to the peak strength of rocks. Based on a large amount of experimental data, Fujii et al.[5] analyzed the relationship between micro-parameters of mineral crystals and the macro-mechanical characteristics of rocks. Ündül et al.[6,7] studied the relationship between mineral crystal compositions and rock strength, finding a positive correlation between plagioclase mineral crystal content and the initiation stress and compressive strength of rocks, and noting the impact of the microstructure of mineral crystals. Merrian et al.[8] observed that rocks with higher quartz content, due to their structural differences, have a tensile strength inversely proportional to the quartz

[1]State Key Laboratory of Geo-Hazard Prevention and Geo-Environment Protection, Chengdu University of Technology, Chengdu 610059, Sichuan, China. [2]Sichuan Chengnan Expressway Corporation Limited, Chengdu 610000, Sichuan, China. [3]CCCC Highway Consultants Corporation Limited Beijing, Beijing 100010, China. ✉email: zhqh@163.com

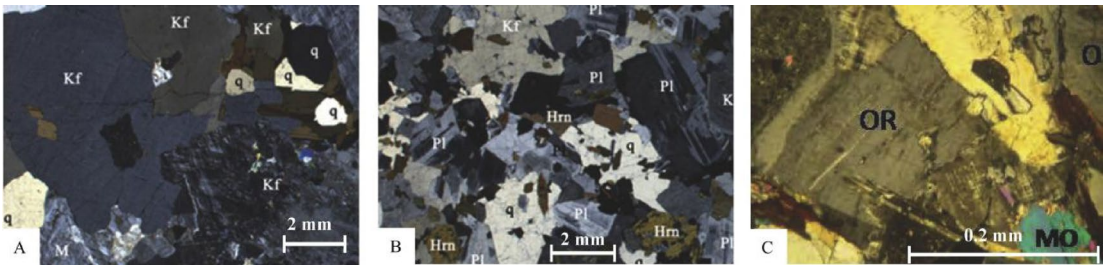

Fig. 1. Granite mineral crystal microstructure[1,2].

content. Thus, the characteristics of mineral crystal composition in rocks significantly affect their mechanical properties. However, obtaining the microstructure inside rocks often damages the samples themselves, making such research very challenging in laboratory experiments[9–12].

Compared to laboratory experiments, numerical simulation methods have significant advantages in analyzing the internal damage and failure processes of rocks, as well as the fracture characteristics at the crystal scale[13,14]. For instance, Lan et al.[13] used Universal Distinct Element Code(UDEC) to analyze the impact of heterogeneity on stress distribution and crack propagation in rock failure. Wang et al.[15] employed 3-Dimensional Distinct Element Code (3DEC)to study the effect of particle properties on the macro-mechanical behavior of samples, finding that due to the particle chain effect, the volumetric strain of rigid particles is not significant, and elastic particles make it difficult to capture the deformation of brittle rocks. Potyondy et al.[16,17] were the first to establish a complex rock model based on granular structure in PFC, namely the GBM model, enabling the quantification and modeling of mineral crystal composition and size. This model can reproduce the interactions between crystals and also simulate the granular mechanical behavior within mineral crystals. The establishment of the GBM model has greatly facilitated research on the impact of microstructure on the mechanical behavior of rocks[18,19].

In the two-dimensional aspect, Li et al.[20] used the PFC-GBM model to establish uniaxial and Brazilian split tests, analyzing the mechanical properties of rocks with different mineral crystal sizes and distributions. They suggested that fractures primarily occur at the boundaries of mineral crystals, and there is a positive correlation between the size of mineral crystals and compressive strength. Li et al.[21–23] utilized digital image processing technology to scan rock mineral crystals, simulating the microstructure of rocks. They discussed the effects of mineral crystal shape, size, and different strain rates on the process of micro-crack formation in rocks. The two-dimensional models lack a degree of freedom compared to actual samples and have certain limitations in explaining three-dimensional physical phenomena in nature. On the three-dimensional scale, Wang et al.[24] proposed a method to import Voronoi diagrams into PFC software to establish the PFC-GBM model. They believed that crystal cohesion and particle count have a significant impact on compressive strength and proposed a calibration method for crystal strength. However, Wang et al.[24] did not differentiate among groups of mineral crystal particles, they calibrated all intra-crystal contacts using the same bonding model. Zhang et al.[25] analyzed the effect of mineral crystal size on the destabilization and failure process of rocks, suggesting that tensile failure is the primary mode of damage, and grain boundary failure is the dominant pattern. Li et al.[26] studied the micro-mechanical properties of rock salt at the granular scale, finding that as axial stress increases, tensile cracks between grains transition to shear cracks. These studies validate the feasibility of using the PFC-GBM model to simulate the effects of mineral crystal compositions on the mechanical properties of hard rocks like granite and rock salt, but there has been less analysis on soft rocks such as mudstone.

Due to various factors such as the diagenetic environment and period, the structure of mudstone and the composition of its mineral crystals differ significantly. Numerous studies have shown that these differences in mudstone's mineral crystal composition are mainly reflected in the content of clay mineral crystals. To investigate the impact of the proportion and structural changes of mineral crystal compositions on the failure mechanism of mudstone, this paper first conducts laboratory experiments to determine the mechanical properties of mudstone. The PFC-GBM model of mudstone is then realized through parameter calibration, with the sample contact model divided into two types: intra-crystal contacts and grain boundary contacts. This study analyzes the trends in failure morphology, crack development, and acoustic emission characteristics under uniaxial compression, thereby investigating the failure mechanism of heterogeneous mudstone.

Mineral crystal model theory and implementation process

Introduction to the PFC-GBM model

Potyondy et al.[16,17] developed the PFC-GBM method by constructing a Voronoi tessellation using the built-in geometry command function of the PFC software. The geometry tessellate Voronoi command generates Thiessen polygonal meshes, with each polygon mesh representing a mineral crystal. Within each mineral crystal, a Parallel Bonded Model (PBM) is applied, while the Smooth Joint Model (SJM) is assigned at interfaces between mineral crystals, enabling the modeling of micro-scale mineral crystal structures in heterogeneous rocks (Fig. 2). The general modeling procedure of the PFC-GBM includes the following four steps (Fig. 2): (1) Generation of equivalent spherical particles for mineral crystals: Particles with varying sizes are generated based on the dimensions and proportions of mineral crystals. Each particle contains at least two contact points and represents the initial formation of a mineral crystal. (2) Intercrystalline pore mesh division: Different meshes are

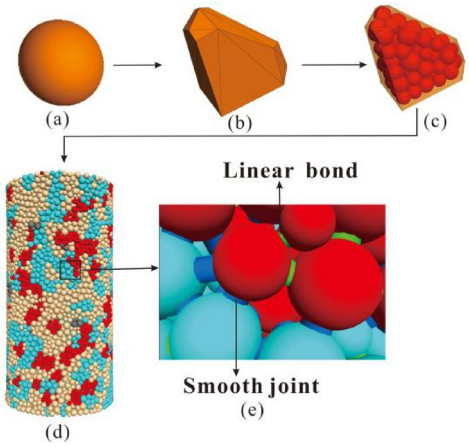

Fig. 2. PFC-GBM modeling process.

created according to particle sizes and interparticle voids. (3) Secondary particle filling deployment: A second particle-based model is constructed using smaller-sized particles to fill various meshes. (4) Group assignment of mineral components: Particles are grouped according to mineral composition to form the final specimen. As shown in Fig. 2e, bonding between particles of the same mineral crystal type utilizes the Parallel Bonded Model (indicated by red bonds), whereas bonding between particles of different mineral types employs the Smooth Joint Model (indicated by blue bonds).

Establishment of the mudstone model

The study area is located in Suining City, Sichuan Province, China, primarily encompassing the Upper Jurassic Suining Formation, consisting mainly of mudstone and sandstone. This research focuses specifically on mudstone, characterized by a brownish color, a mud-rich matrix, medium to thick layering, and poorly developed joint fissures. X-ray diffraction (XRD) analysis of typical mudstone samples indicates that the mineral composition predominantly includes quartz, albite, clay minerals (such as illite, chlorite, kaolinite, montmorillonite, etc.), and trace amounts of hematite and siderite, which can be considered negligible. The respective proportions of quartz minerals, feldspar minerals, clay minerals, and other minerals are 38.4%, 16.5%, 41.9%, and 3.2%. Additionally, standard cylindrical specimens measuring 50 mm × 100 mm were utilized to obtain mechanical parameters, preparing the foundation for subsequent parameter calibration.

Micro-parameter calibration

To accurately simulate laboratory test data, this study employs a trial-and-error method to construct a 1:1 scale model of actual rock specimens using PFC3D software. In the numerical simulation of the uniaxial compression test, it is necessary to first establish the walls and create a closed region with four walls. The positions of the walls are fixed, and particles are generated within the closed region. Using time step iterations, the particles reach equilibrium, after which the left and right walls are deleted. The particles are then assigned cohesive parameters, and a certain velocity is applied to the walls to exert pressure on the sample until it fails. The loading speed of the walls is determined by considering both the indoor tests and the numerical simulation to match the failure speed observed in Yang's experiments. In this paper, the loading speed is set to 0.05 m/s.

By replicating the stress-strain curves and failure patterns observed in laboratory tests, numerical simulation results can effectively reflect the characteristics of laboratory experiments (Fig. 3). As illustrated in Fig. 3 (Single sample mechanical characteristic curve), there is notable similarity between numerical and experimental outcomes, both in stress-strain behavior and failure modes. Table 1 compares the mechanical parameters obtained from laboratory tests and numerical simulations, demonstrating that the error between them is controlled within 15%, confirming that the numerical simulations accurately represent the actual rock conditions. Summarizing the research of many scholars[25,27–29], the strength order of each mineral crystal is: Quartz mineral crystals > Feldspar mineral crystals > Clay mineral crystals > Other types of mineral crystals, Specific parameters are detailed in Table 2, which lists the relevant parameters for the parallel bonded model within the PFC software.

Results analysis

Evolution of acoustic emission patterns

Mudstone failure occurs progressively rather than instantaneously. In the numerical simulation conducted in this study, the generation of internal micro-cracks within the mudstone corresponds to acoustic emission (AE) events. By monitoring and recording cracks over a period, the process of AE occurrence can be determined. To analyze the relationship among stress, strain, the number of acoustic emission events, and cumulative acoustic emission events at different stages of mudstone deformation, the evolutionary curves illustrated in Fig. 4 were established.

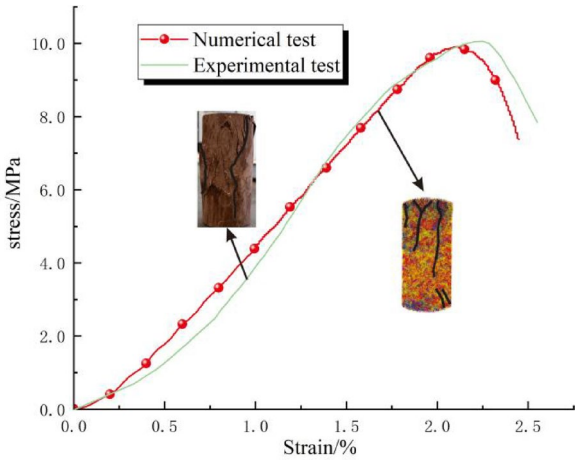

Fig. 3. Calibration of mudstone laboratory test and numerical simulation parameters.

Microscopic parameters	Numerical simulation	Indoor test	Different(%)
Uniaxial compressive strength(MPa)	9.91	10.14	2.26
Tensile strength(MPa)	0.34	0.29	14.71
Elastic modulus(GPa)	2.75	2.56	6.91
Poisson's ratio	0.283	0.271	4.24
Cohesion(MPa)	1.42	1.55	8.38
Friction angle(°)	23	25	8.00

Table 1. Comparison of numerical simulation and indoor test parameters.

Parameter	Quartz-type minerals	Feldspar-type minerals	Clay-type minerals	Other types of minerals	Inter-mineral crystal parameters
Mineral volume fraction	0.384	0.165	0.419	0.032	
Mineral crystal size d/mm	1.896 ± 1	2.296 ± 1	1.696 ± 1	1.296 ± 1	
Particle size range d/mm	0.96–1.92				
Density /(Kg·m^{-3})	2650	2600	2850	2850	
Linear stiffness ratio E/GPa	5.7	4.5	3.0	3.4	3
Parallel bond stiffness Ratio	5.7	4.5	3.0	3.4	3
Linear elastic modulus/GPa	0.8	0.9	1.1	1.3	1.5
Parallel bond elastic modulus/GPa	0.8	0.9	1.1	1.3	1.5
Tensile strength/MPa	16	13	7	7	3.8
Bond strength/MPa	11	8	5	4	3.5
Friction angle/°	23	28	15	13	33

Table 2. Micro-parameters of mudstone PFC-GBM model.

According to the analysis of Fig. 4, combined with the evolution patterns of stress-strain curves and acoustic emission (AE) events, the mechanical response characteristics of mudstone under uniaxial compression testing can be divided into four stages: (1) Elastic deformation stage (OA): With continuous axial loading, the stress-strain curve shows a downward bending trend. No acoustic emission events occur, indicating that the mudstone does not experience irreversible deformation. (2) Stable crack propagation stage (AB): The stress-strain curve approximates a straight line, and cumulative AE events steadily increase. Cracks are mainly located at the ends of the mudstone specimen, generating a small number of cracks within clay mineral crystals and intercrystalline cracks between mineral crystals. Due to relatively few AE events, the AE event number curve nearly coincides with the coordinate axis. (3) Unstable crack propagation stage (BC): The stress-strain curve exhibits an upward bending trend, and the cumulative AE events curve also increases notably, indicating accelerated mudstone failure. Microcracks extend toward the central region of the mudstone and start clustering. Near a strain of approximately 2.0, numerous AE events occur, causing the cumulative AE event curve to increase almost vertically. A substantial number of AE events occur before the peak strength is reached, signifying significant damage in the mudstone, although the specimen still retains a certain residual strength. (4) Post-peak stage

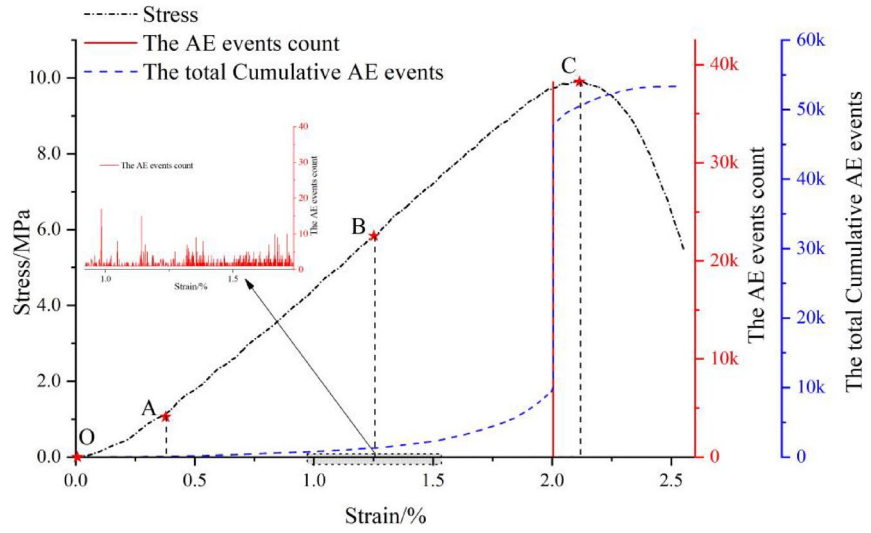

Fig. 4. Evolution of mudstone stress, The AE events count, and the total cumulative AE with strain.

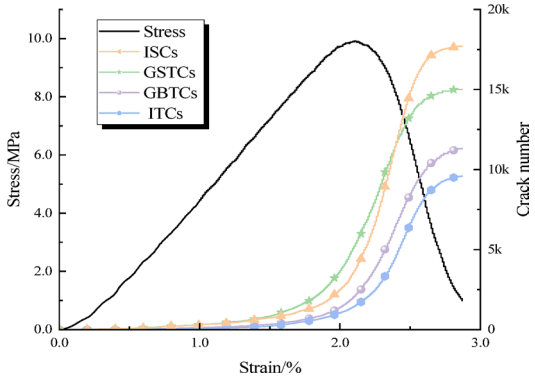

Fig. 5. Evolution trend of mudstone stress-strain and cracks within and between mineral crystals.

(after point C): Mudstone reaches peak strength, and subsequently, strength decreases rapidly. AE events become fewer, and the cumulative AE event curve's growth rate diminishes and gradually stabilizes. Clusters formed during the BC stage continue aggregating, resulting in the formation of larger clusters and subsequently leading to the development of macro-scale fracture surfaces. Based on the insights into the rock failure process proposed by Asemi et al.[30] and the data presented in Fig. 4, the crack initiation strength and peak strength of the mudstone are determined as 1.57 MPa and 9.91 MPa, respectively.

Crack evolution patterns

To analyze crack evolution during mudstone failure, programming was performed on the software's internal fracture file using the FISH language. Initially, contacts among mineral components were grouped, then cracks within each mineral component were classified into shear and tensile cracks. Finally, these cracks were statistically analyzed to monitor their respective evolution trends. Fig. 5 illustrates the relationships among stress, strain, internal tensile cracks within crystals (ITCs), internal shear cracks within crystals (ISCs), intergranular tensile cracks (GBTCs), and intergranular shear cracks (GSTCs). With increasing compressive strength, mineral crystals first exhibit failure through tensile cracking, followed by a gradual increase in shear cracks. As damage progresses, slip occurs between mineral crystals, subsequently increasing intergranular cracking. After reaching a strain of approximately 1.0, intergranular shear cracks significantly increase and dominate crack formation until mudstone failure. Post-peak strength, internal shear cracks within mineral crystals rapidly increase, becoming dominant. Overall, the order of crack quantities after mudstone failure is ISCs > GSTCs > GBTCs > ITCs. Based on these observations, the mudstone failure process can be described as follows: As axial load increases, mineral crystals initially undergo damage, followed by slip between crystals resulting in extensive shear cracks. After reaching peak strength, shear cracks within the mineral crystals primarily drive the failure process. After the complete failure of the mudstone, shear cracks account for 61.3% of the total cracks.

Figure 6 illustrates the evolution trends of stress, strain, cracks within quartz mineral crystals (CQM), feldspar mineral crystals (CFM), clay mineral crystals (CCM), other mineral crystals (IC), and intercrystalline

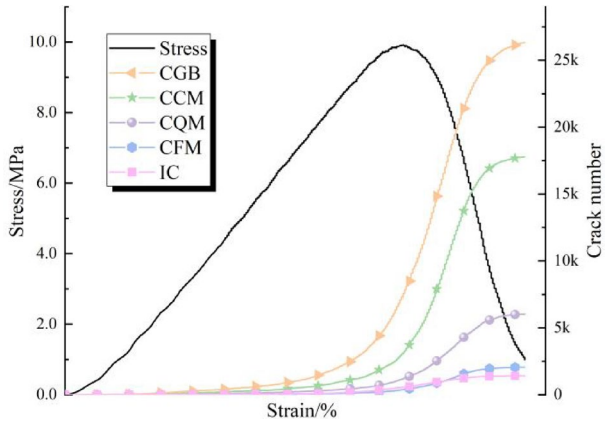

Fig. 6. Stress, strain, and the evolution relationship of cracks in different mineral crystals.

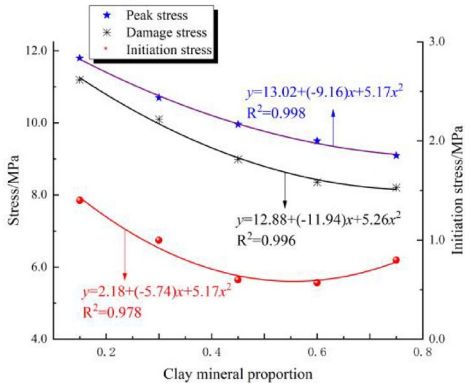

Fig. 7. Analysis of the impact of different clay mineral crystals on the mechanical properties of mudstone.

cracks (COM). With increasing axial load, clay mineral crystals are the first to experience damage and form cracks, followed by intercrystalline movement generating additional cracks. Subsequently, other mineral crystals progressively fail. After mineral crystal damage reaches a certain threshold, intercrystalline cracks rapidly increase, surpassing the development of clay mineral cracks. This phenomenon primarily occurs due to the relatively high content of clay minerals combined with their weak intercrystalline contacts, resulting in rapid crack proliferation upon relative movement between crystals. These findings indicate that stress concentration and redistribution continuously occur within heterogeneous rock during mudstone failure, leading to substantial crack formation due to relative displacements between mineral crystals. Feldspar and other mineral crystals exhibit fewer cracks, mainly because feldspar, despite its relatively high proportion, has greater strength, whereas other minerals have lower proportions and lower strengths. Crack development trends in these two categories are thus comparatively similar. After complete failure of the mudstone, intercrystalline cracks represented 52.7% of the total cracks.

The influence of different clay mineral crystal contents on the deformation mechanism of mudstone

To investigate the influence of clay mineral content on the mechanical properties of mudstone, this study set the proportions of clay minerals at 0.15, 0.30, 0.45, 0.60, and 0.75, respectively. Figure 7 illustrates the variation patterns of peak strength (σ_{ci}), damage strength (σ_{cd}), and cracking strength (σ_p) with different clay mineral contents (where clay mineral proportion is represented by h).

The results indicate that both peak strength and damage strength of mudstone decrease as clay content increases, exhibiting an initially rapid reduction followed by a gradual slowing down. This decreasing trend can be attributed to the lower strength of clay minerals compared to quartz and feldspar minerals. It also suggests that beyond a certain proportion, additional clay minerals have a diminishing effect on mudstone strength. Crack initiation stress shows a trend of initially decreasing and subsequently increasing. Furthermore, curve fitting was conducted on the three relationships presented in the figure. The results demonstrate significant quadratic relationships between strain and peak stress, damage stress, and crack initiation stress, with correlation coefficients (R^2) exceeding 0.98. The fitting equations are provided as Eq. (1) to (3). These equations enable more accurate predictions of mudstone mechanical properties at varying clay mineral contents.

$$\sigma_{ci} = 13.02 + (-9.16)\, h + 5.17h^2 \tag{1}$$

$$\sigma_{ci} = 12.88 + (-11.94)\, h + 5.26h^2 \tag{2}$$

$$\sigma_{ci} = 2.18 + (-5.74)\, h + 5.17h^2 \tag{3}$$

In recent years, moment tensor inversion methods have been used to analyze the mechanical mechanisms, fracture types, and morphologies of internal micro-fractures in rocks, yielding rich results. Hudson et al.[31] proposed an analytical method defining the moment tensor with two parameters, T and k. T represents the deviatoric component of the source, ranging from − 1 to + 1, representing a pure linear vector dipole (CLVD) that compensates in the positive direction and passes through the origin for pure double-couple, with a positive linear vector dipole (LVD+) representing linear tensile fracturing and a negative linear vector dipole (LVD-) representing linear shear fracturing. k represents the isotropic component of the source, ranging from + 1 for uniform expansion types to -1 for uniform compression types. Assuming M1 > M2 > M3 are the three eigenvalues of the moment tensor, the T and k parameters can be represented as (Hudson)[31]:

$$T = \frac{2M_2'}{\max\left(\left|M_2'\right|, \left|M_3'\right|\right)} \tag{4}$$

$$K = \frac{M_{ISO}}{\left|M_{ISO} + \max\left(\left|M_1'\right|, \left|M_3'\right|\right)\right|} \tag{5}$$

In the formula; $M_{ISO} \rightarrow \frac{1}{3} tr\,(M)$;$M_1', M_2', M_3'$— characteristic value of the deviatoric component of the moment tensor.

As shown in Fig. 8, the T-k diagram for mudstone with different clay mineral crystal contents is presented. The T-k value points of the mudstone with varying clay mineral crystals mainly concentrate near the line y=-x/2. This includes a large number of linear tensile fractures, linear shear fractures, double couple fractures, and mixed fracture events. The distribution of T-k value points in the first and third quadrants, albeit limited, indicates that the numerically simulated mudstone is an anisotropic medium, further validating that the PFC-GBM model can accurately simulate actual mudstone. When the content of clay mineral crystals is low, the number of LVD- events is significantly greater than LVD + events. As the clay content increases, events near LVD + gradually become more numerous. However, even when the clay content is 0.75, the number of LVD + events remains smaller than the negative pole, but with an increasing content of clay mineral crystals, linear tensile fractures gradually increase. Linear tensile fractures are always less than linear shear fractures, indicating that the failure of mudstone is predominantly linear shear failure. When the proportion of clay mineral crystals ranges from 0.3 to 0.6, there are a few CLVD events, but there are no such events in the rest, indicating that the failure of this type of mudstone is more complex.

By programming with the FISH language, the number of contacts between different mineral crystals after mudstone failure was monitored, and a three-dimensional fabric rose diagram (Fig. 9) was generated to analyze the distribution and quantity of cracks after mudstone failure. Figure 9 shows that with an increase in clay mineral

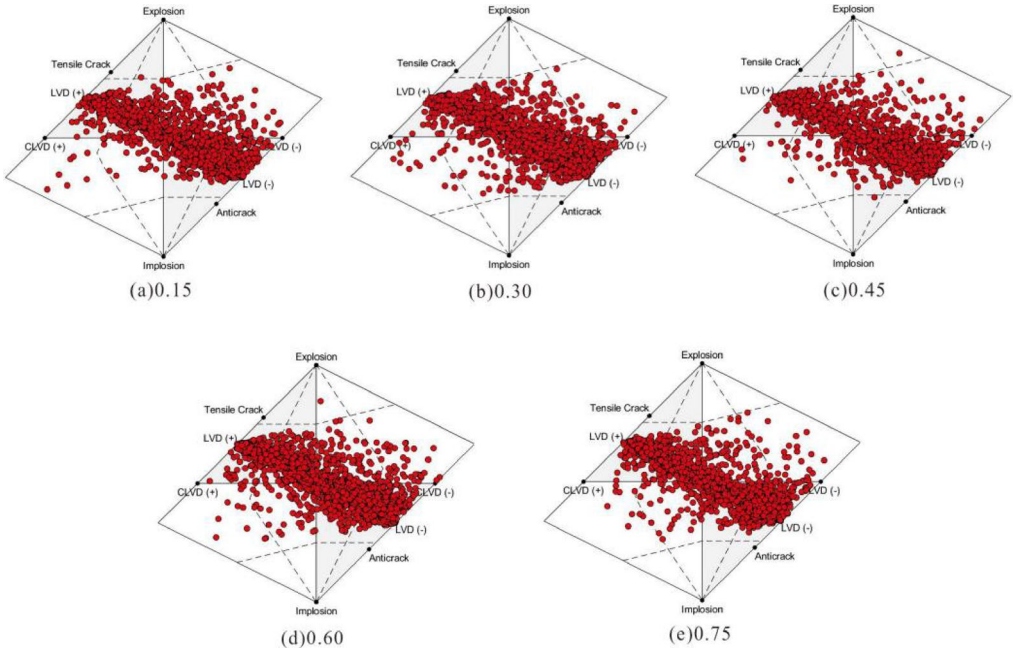

Fig. 8. Impact of different proportions of clay minerals on the T-k diagram of mudstone.

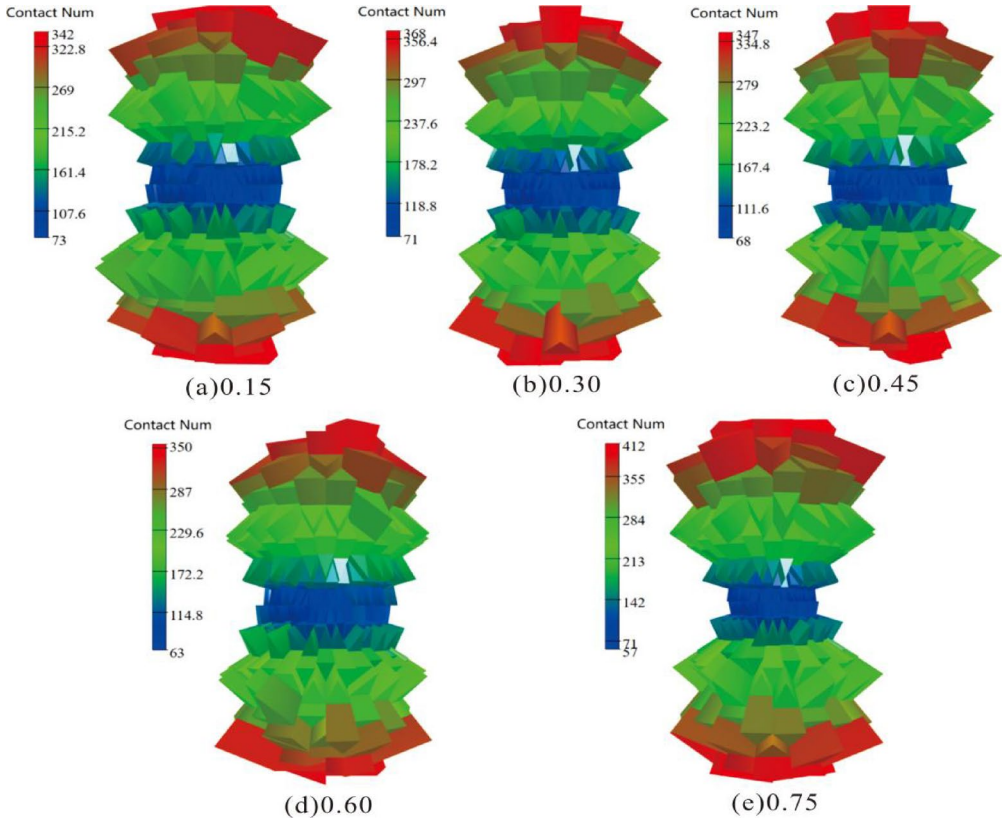

Fig. 9. Three-dimensional rose diagram of mudstone destruction with different proportions of clay minerals.

content, the number of contacts within the mudstone initially increases, then decreases, and finally increases again at the top, bottom, upper-middle, and lower-middle parts of the mudstone specimen. Conversely, the number of contacts in the central part of the mudstone gradually decreases. This indicates that as clay mineral content increases, substantial damage initially occurs at the top of the mudstone specimen. Before significant central damage can develop, the mudstone loses strength, leading to termination of loading. This occurs because when the proportion of clay minerals is relatively low, other mineral crystals with higher strength resist failure, prompting relative displacement between mineral crystals and allowing damage to propagate toward the central region. However, when the clay mineral proportion is high, rapid damage occurs at both the top and bottom regions of the mudstone, causing a swift loss of structural integrity and strength.

Impact of mineral sizes

To analyze the influence of mineral crystal size on the deformation mechanisms of mudstone, this study varied the number of mineral crystal particles within the same spatial region to represent different mineral crystal sizes. Specifically, particle counts of 25,000, 20,000, 15,000, 10,000, 5,000, and 500 (referred to as 2.5, 2.0, 1.5, 1.0, 0.5, and 0.05 in Fig. 10, respectively) were used. Red particles represent quartz minerals, purple particles represent feldspar minerals, yellow particles indicate clay minerals, and black particles depict other minerals. This approach effectively characterizes variations in mineral crystal size.

Simulation results showed similar uniaxial compressive strengths for mudstones with different mineral crystal sizes, ranging between 9.91 and 10.06 MPa. However, significant differences were observed in failure patterns associated with varying mineral crystal sizes. As shown in Fig. 11 (with red indicating internal crystal cracks and black representing intercrystalline cracks), increasing mineral crystal size reduced cracks at the top and bottom regions of the specimen, allowing cracks to propagate progressively toward the center, resulting in more continuous overall damage. Specimens with 25,000 particles exhibited cracks concentrated mainly at specimen ends, with damage in the central region primarily due to relative movement between crystals. Conversely, specimens with 500 particles showed less damage at the bottom, but internal and intercrystalline damage was evident in the middle. This implies that smaller mineral crystals allow extensive damage at specimen ends, with central crystals mostly experiencing relative displacement, whereas larger crystals facilitate rapid crack propagation from ends to the center, creating continuous fractures.

Figure 12 illustrates the crack evolution in mudstone specimens with varying mineral crystal sizes. Figure 12a compares internal and intercrystalline crack numbers after failure. As mineral crystal size decreased, internal cracks initially increased and then decreased, whereas intercrystalline cracks increased consistently. When particle counts exceeded 20,000, crystal size had minimal influence on crack numbers, suggesting that reducing mineral crystal size primarily promotes relative displacement between different crystals under loading, inducing

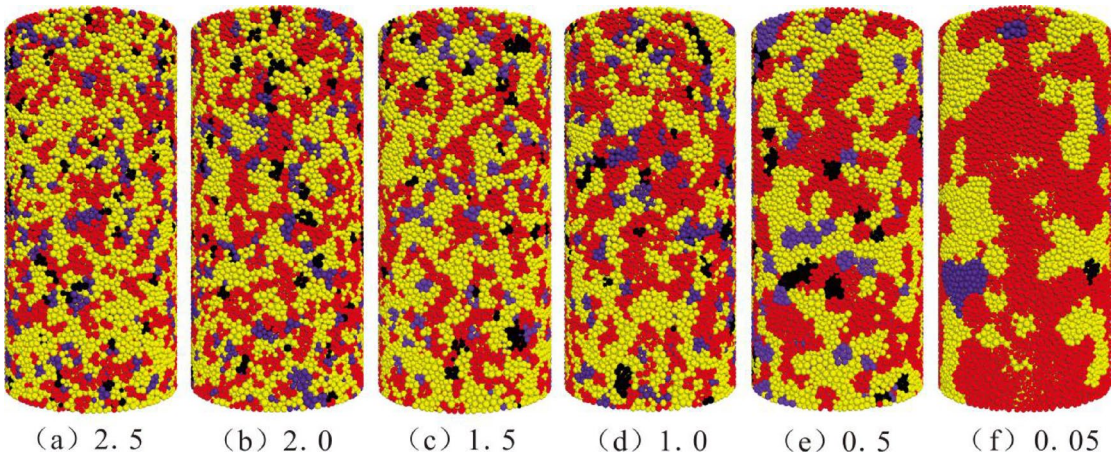

Fig. 10. Mudstone samples with different mineral sizes

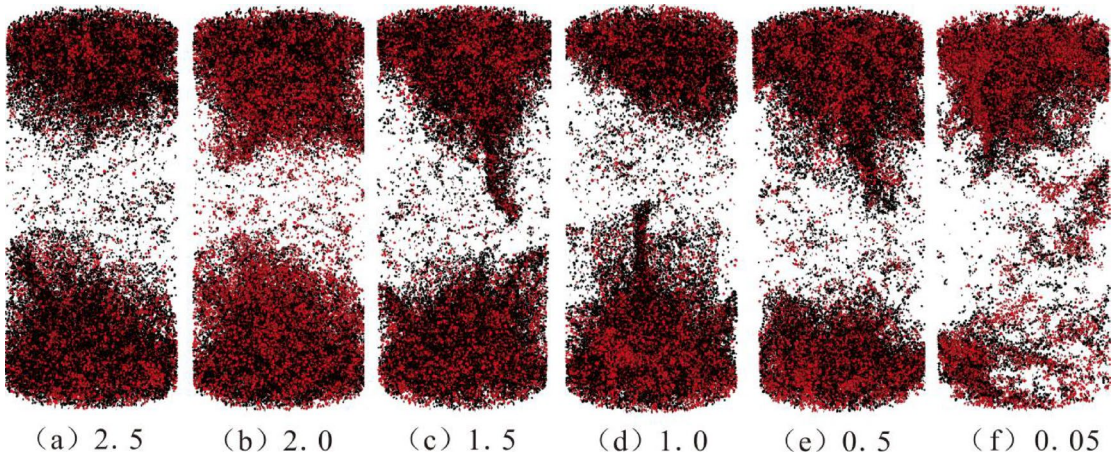

Fig. 11. Distribution map of failure cracks in mudstone samples with different mineral sizes.

shear and tensile cracks, while having minimal impact on crystals themselves. The size of mineral crystals primarily affects the generation of intercrystalline cracks, with the proportion of such cracks rising from 25.3 to 51.5%. Figure 12b demonstrates trends in shear and tensile crack quantities and the proportion of tensile cracks with changing crystal sizes. The total number of cracks initially increased and then decreased with decreasing crystal size, and shear cracks consistently outnumbered tensile cracks. Additionally, the proportion of tensile cracks decreased as crystal size diminished.

Conclusion

This paper, through laboratory experiments, obtains the constitutive relationship of mudstone and uses the PFC-GBM model to simulate the heterogeneous structure of mudstone mineral crystals. It analyzes the characteristics of mudstone failure process, the impact of different clay mineral crystals, and different mineral crystal sizes on the mudstone failure process. The main conclusions are as follows:

(1) By calibrating the stress-strain curve and failure mode of mudstone, it is believed that the PFC-GBM model can effectively simulate the structure and heterogeneous characteristics of mudstone mineral crystals. Additionally, the model can simulate the evolution of cracks and acoustic emission characteristics during the mudstone failure process, making it an effective research method.

(2) A surge in the number of acoustic emission events of mudstone occurs before the compressive strength of mudstone. During the failure process of mudstone, clay-type mineral crystals in the mineral crystals are the first to fail, followed by failure between mineral crystals. ISCs generate the largest number of events, followed by grain boundary cracks.

(3) As the clay content in mudstone increases, both the peak stress and damage stress show a decreasing trend, while the initiation stress first decreases then increases. These three trends were fitted, and through the T-K diagram, it is shown that the failure of mudstone is mainly characterized by linear shear failure, occurring more at the bottom and top of the sample.

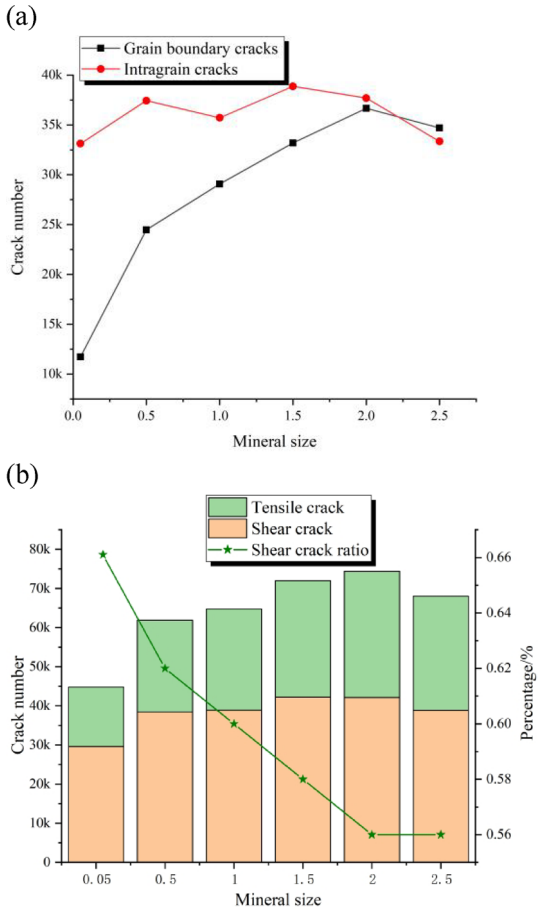

Fig. 12. The impact of different mineral sizes on the number of cracks after the failure of mudstone.(**a**) The impact of mineral size on the number of cracks within and between mineral crystals in mudstone, (**b**) The impact of mineral size on the number of tensile and shear cracks after the failure of mudstone.

(4) As the size of the mineral crystals increases, the failure of mudstone gradually penetrates towards the interior, forming overall failure. Tensile failure gradually becomes the predominant mode of damage. The size of the mineral crystals mainly affects the relative movement between mudstone mineral crystals, leading to significant changes in the cracks between mineral crystals.

Data availability

All data generated or used during the study are included in the submitted article.

Received: 30 December 2024; Accepted: 8 May 2025
Published online: 16 May 2025

References

1. Tuğrul, A. & Zarif, I. H. Correlation of mineralogical and textural characteristics with engineering properties of selected granitic rocks from Turkey. *Eng. Geol.* **51**, 303–317 (1999).
2. Keikha, T. & Keykha, H. A. Correlation between mineralogical characteristics and engineering properties of granitic rocks. *Electron. J. Geotech. Eng.* **18**, 4055–4065 (2013).
3. Hallbauer, D. K., Wagner, H. & Cook, N. G. W. Some observations concerning the microscopic and mechanical behaviour of quartzite specimens in stiff, triaxial compression tests. *Int. J. Rock. Mech. Min.* **10**, 713–726 (1973).
4. Wong, R. H. C., Chau, K. T. & Wang, P. Microcracking and grain size effect in yuen long marbles. *Int. J. Rock. Mech. Min. Sci. Geomech. Abstr.* **33**, 479–485 (1996).
5. Fujii, Y., Takemura, T., Takahashi, M. & Lin, W. Surface features of uniaxial tensile fractures and their relation to rock anisotropy in Inada granite. *Int. J. Rock. Mech. Min.* **44**, 98–107 (2007).
6. Ündül, Ö., Amann, F., Aysal, N. & Plötze, M. L. Micro-textural effects on crack initiation and crack propagation of andesitic rocks. *Eng. Geol.* **193**, 267–275 (2015).
7. Ündül, Ö. Assessment of mineralogical and petrographic factors affecting petro-physical properties, strength and cracking processes of volcanic rocks. *Eng. Geol.* **210**, 10–22 (2016).
8. Merriam, R., Rieke, I. I. I., Kim, Y. C. & H. H. & Tensile strength related to mineralogy and texture of some granitic rocks. *Eng. Geol.* **4**, 155–160 (1970).
9. Peng, J., Wong, L. N. Y. & Teh, C. I. Influence of grain size heterogeneity on strength and microcracking behavior of crystalline rocks. *J. Geophys. Res: Sol Ea.* **122**, 1054–1073 (2017).

10. Liu, G., Cai, M. & Huang, M. Mechanical properties of brittle rock governed by micro-geometric heterogeneity. *Comput. Geotech.* **104**, 358–372 (2018).
11. Lakirouhani, A., Asemi, F., Zohdi, A., Medzvieckas, J. & Kliukas, R. Physical parameters, tensile and compressive strength of dolomite rock samples: influence of grain size. *J. Civ. Eng. Manag.* **26**, 789–799 (2020).
12. Lakirouhani, A., Zohdi, B. M., Medzvieckas, J. & A. & Physical and mechanical properties of sandstones from Southern Zanjan, north-western Iran. *Baltica* **35**, 23–36 (2022).
13. Lan, H., Martin, C. D. & Hu, B. Effect of heterogeneity of brittle rock on micromechanical extensile behavior during compression loading. *J. Geophys. Res: Sol Ea.* **115**, B01202 (2010).
14. Nicksiar, M. & Martin, C. D. Factors affecting crack initiation in low porosity crystalline rocks. *Rock. Mech. Rock. Eng.* **47**, 1165–1181 (2014).
15. Wang, X. & Cai, M. A comprehensive parametric study of grain-based models for rock failure process simulation. *Int. J. Rock. Mech. Min. Sci.* **115**, 60–76 (2019).
16. Potyondy, D. O. The bonded-particle model as a tool for rock mechanics research and application: current trends and future directions. *Geosystem Eng.* **18**, 1–28 (2015).
17. Potyondy, D. O. & Cundall, P. A. A bonded-particle model for rock. *Int. J. Rock. Mech. Min. Sci.* **41**, 1329–1364 (2004).
18. Saadat, M. & Taheri, A. A numerical approach to investigate the effects of rock texture on the damage and crack propagation of a pre-cracked granite. *Comput. Geotech.* **111**, 89–111 (2019).
19. Zhou, J., Lan, H., Zhang, L. & Song, W. Novel grain-based model for simulation of brittle failure of Alxa porphyritic granite. *Eng. Geol.* **251**, 100–114 (2019).
20. Li, G., Liu, S. Q., Ma, F. S. & Guo, J. A multilevel parallel bonded-grain based model (Multi Pb-GBM) accounting for microstructure failures of typical crystalline rocks. *Bull. Eng. Geol. Environ.* **81**, 1–14 (2022).
21. Li, X. F., Li, X., Li, H. B., Zhang, Q. B. & Zhao, J. Dynamic tensile behaviours of heterogeneous rocks: the grain scale fracturing characteristics on strength and fragmentation. *Int. J. Impact Eng.* **118**, 98–118 (2018).
22. Li, X. F., Zhang, Q. B., Li, H. B. & Zhao, J. Grain-Based discrete element method (GB-DEM) modelling of Multi-scale fracturing in rocks under dynamic loading. *Rock. Mech. Rock. Eng.* **51**, 3785–3817 (2018).
23. Li, X. F., Li, H. B. & Zhao, J. Transgranular fracturing of crystalline rocks and its influence on rock strengths: insights from a grain-scale continuum–discontinuum approach. *Methods Appl. Mech. Eng.* **373**, 113462 (2021).
24. Wang, Z. H., Yang, S. L., Liang, H. T., Yue, S. X. & Guo, L. A 3D Voronoi clump based model for simulating failure behavior of brittle rock. *Eng. Fract. Mech.* **248**, 107720 (2021).
25. Zhang, T., Yu, L. & Wu, B. Influence of grain-to-particle size ratio on the tensile mechanical response of granite based on a novel three-dimensional grain-based model. *Eng. Fract. Mech.* **259**, 108161 (2022).
26. Li, H. et al. A 3D grain-based model for simulating the micromechanical behavior of salt rock. *Rock. Mech. Rock. Eng.* **53**, 2819–2837 (2020).
27. Hofmann, H., Babadagli, T. & Zimmermann, G. A grain based modeling study of fracture branching during compression tests in granites. *Int. J. Rock. Mech. Min. Sci.* **77**, 152–162 (2015).
28. Peng, J., Wong, L. N. Y., Teh, C. L. & Li, Z. H. Modeling micro-cracking behavior of Bukit Timah granite using grain-based nodel. *Rock. Mech. Rock. Eng.* **51**, 135–154 (2018).
29. Zhang, Y., Wong, L. N. Y. & Chan, K. K. An extended grain-based model accounting for microstructures in rock deformation. *J. Geophys. Res: Sol Ea.* **124**, 125–148 (2019).
30. Asemi, F., Lakirouhani, A. & A Zohdi, N. A new rock brittleness index based on crack initiation and crack damage stress thresholds. *Int. J. Geomech.* **24**, 11–112 (2024).
31. Hudson, J. A., Pearce, R. G. & Rogers, R. M. Source type plot for inversion of the moment tensor. *J. Geophys. Res.* **94**, 765–774 (1989).

Acknowledgements

This work was supported by the National Key R&D Program of China [grant number 2011CB013501], the Sichuan Transportation technology project [grant number 2021-ZL-03].

Author contributions

B.W. and Q.Z. wrote the main manuscript text. B.W. and G.L. prepared Figs. 1, 2, 3, 4, 5, 6, 7, 8 and 9, and Tables 1 and 2. B.L. and L.L. prepared Figs. 10, 11 and 12. All authors reviewed the manuscript.

Declarations

Competing interests

The authors declare no competing interests.

Additional information

Correspondence and requests for materials should be addressed to Q.Z.